HJF
Version v13d
November 25, 2024

A Slit Laminar MCP Using Polyimide Substrates

Economical Micro-Channel Plate Construction Using Kapton Tape and Advanced Additive Processes

Claudio Bastiani-Fonck, Camden Ertley, Henry Frisch, Michael Foley, Oliver Moreno, Jinseo Park, John Shelton, Peter Scheidt, Soka Suliman, Neal Sullivan, and Richmond Yeung

DRAFT

Abstract

We have recently proposed a method of constructing MCPs from stacked thin laminae, replacing the complex drawing process for forming micro-capillary channels. The Laminar MCP (LMCP) process allows for the first time direct access to the channel surfaces during construction for implementing custom geometries, surface coatings, integrated anodes and dynodes, and possibly active circuitry [1].

We have been considering LMCP designs for several different applications and their associated configurations: 1) conventional MCP-PMTs (the 'ALMCP) for use with a photocathode (i.e. an incoming electron starts the shower) or as the second electron multiplying plate in a chevron MCP-PMT ; and 2) gamma multipliers using Surface Direct Conversion to produce the primary electron in which the LMCP is both converter and multiplier and there is no photocathode and the depth of the shower starting point varies (the 'CLMCP'). Here we focus on identifying materials and construction methods that are promising in terms of cost and volume production without targeting a specific geometry and use.

The first section of the note is intended as a group-maintained reference guide, with tables and figures of candidate lamina materials and properties, gamma absorption cross-sections and absorption lengths, electron range, and efficiencies Critical considerations of performance and robustness for specific applications are noted but not yet addressed.

The next sections of the note describe a laminar MCP with channel geometry shaped like a slit, i.e. the channel width is appreciably greater than the channel-forming gap between lamina. For example, in the simplest form of the slit channel plate, the nominal dimension for the channel depth is 5 microns, and the channel width is large compared to the gap, on the order of an 100-500 microns [1]. The slit geometry allows patterning and functionalization to be done on commercially-available thin substrates using techniques from the rapidly-developing field of advanced additive processes.

The slit design may allow multiple MCP structures on the laminae with concomitant improved time and space resolution by the implementation on each lamina of multiple 50-ohm anode RF transmission lines as horizontal metal traces across all the channels, with the pulse-height, time and position being determined by single-ended or double-ended readout [2]. For example, 4 independent MCPs could be printed in a 'stack', one above the next, each connected to the HV and with its independent anode readout. To reduce the channel count in each MCP while retaining sub-mm resolution,

the anode traces may be organized into sub-modules in which the anodes from multiple laminae are daisy-chained. The anode signal/ground traces can also be implemented purely additively.

We have conducted a search for substrate materials, contacting vendors to get costs for various glass, ceramic, and plastic 1" by 4" laminae. One attractive material seems to be the polyimide Kapton 500 HN from Dupont, which is available on 1000=foot rolls at 0.005" (125 microns) thickness. Kapton is used for flex-circuit board manufacture, allowing commercial photolithography of electrical traces on the substrate before functionalization with resistive/emissive coatings. Kapton is widely used for flexible PC circuit boards employing sophisticated construction techniques, including vias and multilayers that could be used for inter-lamina connections and RF anodes and dynodes. The lower density also translates into a higher efficiency for electrons in the few-hundred keV region, an attribute that is attractive for gamma-ray conversions such as in TOF-PET.

We present a first pass at defining the fabrication steps for the lamina and the LMCP slab. However a full simulation and the ability to make measurements in precision test stands are essential and still not done. In addition, if we chose a substrate other than non-alkali glass, we need to make measurements addressing the serious problem of maintaining long-term (e.g. 20 years) performance ('robustness') in a sealed volume containing non-standard MCP materials.

The slit design may be particularly suited for use in psec-time resolution in shower-preconverters and electromagnetic calorimeters, with examples being LHCb and KOTO in HEP and heavy-quark and baryon identification at the EIC in Nuclear Physics. We have also been exploring the proposition that in TOF-PET the identification and precise localization of the first interaction of each of the primary gammas from e^+e^- annihilation, i.e. the end-points of the LOR, and exploiting the kinematic constraints and timing of successive Compton scatters (the 'Compton chain') can provide significantly higher rejection of in-patient scattering, better spatial resolution, higher efficiency, and better time resolution, than is possible from reconstructing the gamma energy with optical crystals [3]. The technique, dubbed Surface Direct Conversion (SDC) [1], is to convert gammas to a Compton electron inside a Micro-channel Plate photodetector (MCP). However we need to emphasize that the technique depends on understanding and optimizing the secondary emission yield (SEY) of a many-100 keV electron emerging from (not impinging on) the substrate into a channel starting the shower.

The parameters of the LMCP described here are appropriate for surface direct conversion of the 511 keV gamma rays in TOF-PET. The choice of optimizing for a high-impact improvement in Medical Imaging rather than for use in HEP and NP, is driven by societal benefit while also providing the very large market needed to drive commercialization of the LMCP as a robust, economical, and widely available commodity [4, 5].

Contents

1 Introduction

The basic R&D issues have been solved for the production of large-area micro-channel plate photomultipliers (MCP-PMT) with the unique properties of few-hundred-micron space resolution and correlated timing resolution well below the current 10-ps frontier [6, 7]. However, there are still significant challenges to developing an economical high-volume production of robust detectors appropriate for future large neutrino and collider experiments.

The Laminar MCP (LMCP) allows a wide range of choices for the basic parameters of the MCP channels [1]. Here we discuss LMCPs and propose a particular solution in the parameter space of α, β, and γ that define the channels, where α is the depth of the channel, β is the width of the 'wall' between channels, and γ is the width of the channel [1]. The particular solution is a 'slit' channel geometry, in which α is the critical parameter and is as small as field uniformity and manufacturing tolerances allow, β is not critical, needing only to provide a robust and precise inter-lamina spacer, and γ is large compared to α, sized to provide the required resolution for a given application as determined by simulation. There are a number of advantages of the slit geometry, but the dominant one is that we believe it can be implemented with sophisticated features using additive technologies on unmodified commercially-available thin substrates in a number of materials.

The use of 50-ohm microstrip RF transmission lines for high bandwidth low-channel count readout in MCPs is a mature field [8, 9, 10], including multi-GHz capacitively-coupled anodes [11]. The slit design may allow the implementation of similar anode structures on the substrate as an integral part of the additive fabrication process. For example, each slit could have horizontal metal traces across the resistive channels forming multiple 50-ohm anode RF striplines on which the field lines end, and the 50-ohm transmission line anode could consist of a 10-micron-wide trace of 4-micron-thick copper on the lamina front face opposing a wider ground plane on the back of the neighboring lamina 5 microns away. For readout, a transmission line with the far end unterminated would operate in the single-ended 'bounce' mode used with the LAPPD RF anodes [12]. To reduce the channel count while retaining sub-mm resolution, the anode traces of 'sub-modules' of a number of laminae could be daisy-chained into a single folded transmission line connected to a single high-bandwidth 50-ohm electronics channel for multi-sample digitization [13, 14, 13, 15, 16, 17, 18, 19]. The connection from the sub-module to the DAQ system could be done on the ends of the sub-module by contact with an array of pads on the case. All cable or fiber connections would be on the case.

The organization of this note is as follows. Section 2 is a collection of basic physical parameters and figures related to the choice of substrate and coating materials. The 'simple slit' LMCP with channels formed by physical spacers is described in Section 3. For the ALMCP a large OAR can be achieved by one-dimensional funnels ('troughs') at the slit entrance. Section 4 describes integrating RF-stripline anodes into the LMCP structure. Section 5 attempts a preliminary sketch of the lamina fabrication, including patterning the channels, resistive and emissive layers, and HV distribution. Areas of major concern are briefly discussed in Section 6. A brief summation is given in Section 7.

Appendix A serves to archive a proposal for replacing physical walls with closely-spaced narrow 'electrostatic virtual channels' (EVC) and walls (EVW) created by differential electric potentials on conductors under the coatings on the slit surfaces. The underlying technique led to the current proposal of 'pinning' the potential at depths along the channels, essentially making dynodes and supplying current to replenish charge injected into the showers.

2 Material Properties, Gamma Absorption Cross-sections, and Electron Ranges

This section is intended as a repository for numbers, plots, and references that will keep occurring during the detector development.

2.1 Materials and Material Properties

The thickness of a lamina will determine the resolution in at least one transverse dimension in use as a conventional MCP. For the PET application using Surface Direct Conversion, the lamina substrates must be thin enough for the primary electron to have a high probability of reaching a channel wall, while thick enough for robust fabrication and assembly. Additionally the substrate needs to be vacuum compatible, temperature stable up to 200C, and amenable to stable coating. Cost and robustness over time for the finished LMCP will be the ultimate deciders of material and substrate thickness.

Table 1 is a 'working list' of candidate substrate materials. Initially we have focused on materials in stock or on short delivery. Future high-volume orders might justify some effort in optimizing one of these materials or something new.

Material	Composition	Density g/cm^3	$< Z >$	Comment
Polyimide	TBD	1.42	TBD	Kapton HN (Dupont)
PEEK	C19H12O3 (76/8/16%)	1.31	5.9	Curbell Plastics
Ceramic	Al2O3	3.95	14.8	ICE ceramic
D263M	TBD	2.51	TBD	Schott
NIST PbG	O(15%)Si(8%)Pb(75%)	6.22	63.8	fraction by weight

Table 1: Table of candidate substrate materials. $< Z >$ is the atomic number; λ_{PE} is the gamma PhotoElectric absorption length at 511 keV; λ_C is the Compton absorption length; τ^{90} is the lamina thickness for 90% efficiency of wall crossing; τ^{60} the thickness for 60% efficiency.

Table 2 lists quotes from vendors for 4" x 1" x τ substrates, where τ ('tau') is the lamina thickness.

Material	τ (μm)	N#/4"slab	Unit cost Quant 1000	Unit cost 100,000	Cost 4"x1" Slab	Comment
Polyimide	125μm	800	\$0.12	\$0.12	\$96	Dupont 10/31/24
Al2O3	381 μm	263	\$1.62	\$1.32	\$367	ICE 7/9/24
D263M	85-115 μm	2000*	\$0.29		\$580	Thorlabs 9/24/24
D263M	145 μm	690	TBD	TBD	TBD	Schott-RFQ in
D263T	50 μm	2000	TBD	\$41,53	\$83,060	PGO 9/23/24
D263T	100 μm	1000	TBD	\$8.52	\$8,520	PGO
D263T	145 μm	690	TBD	\$7.54	\$6,003	PGO
D263T	210 μm	476	TBD	\$2.11	\$1,005	PGO
PEEK	TBD TBD μm	TBD	TBD	TBD	TBD	Curbell Plastics

Table 2: Vendor quotes on candidate substrate materials in various thicknesses and quantities. The Dupont Kapton cost (Cara Zaiss) does not include special-handling fees for small quantities. The PGO D263T laminae are not ground; the cost for the thinnest glass is dominated by breakage and handling. $*$ The Thorlabs number for D263M is from their web page and is for microscope slide covers that are 1"x 2" so the quantity and total cost have been doubled.

2.2 Gamma Absorption Cross-sections and Absorption Lengths

Figure 1 shows the Compton scattering and photo-electric (PE) absorption cross-sections for 500 keV gamma rays versus atomic number Z. The Compton cross-section is completely dominant for low Z, being comparable to the PE cross-section for lead. However note that the total efficiency will include the efficiency for the Compton electron to propagate from the medium into a channel wall and then to make a shower in the channel by secondary emission.[1]

[1]This number, exiting from rather than impinging on from the outside, does not seem to be well understood but is thought to be small for higher-energy electrons, and so may take substantial effort on the work function and measurements to raise it while staying below the noise limit.

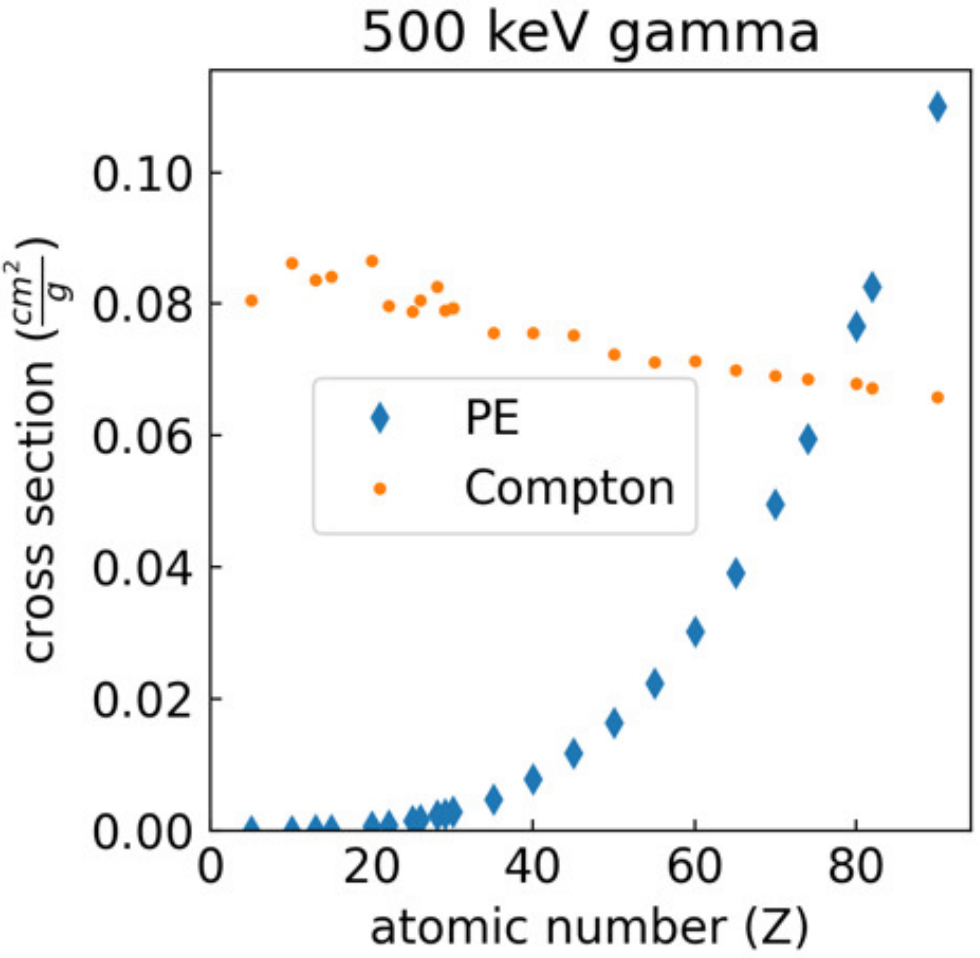

Figure 1: The Compton scattering and photo-electric absorption cross-sections for 500 keV gamma rays versus atomic number Z. The units are cm^2/g; to convert to absorption length in cm multiply by the density ρ in g/cm^3. (Kepler)

2.3 Electron Range Plots

Figure 2 shows the differential distribution in range of electrons in Schott D263M. The ordinate scale is per-cent per mm.

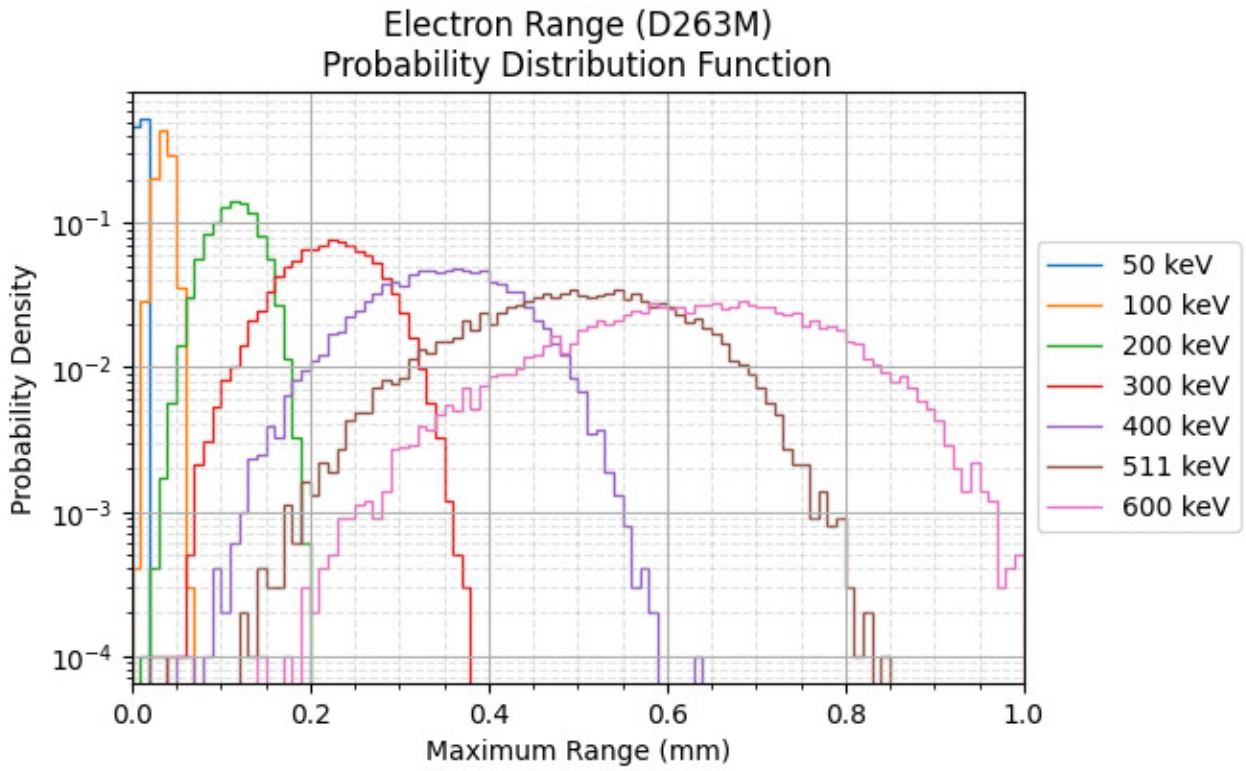

Figure 2: The differential distributions in range of electrons in Schott D263M borosilicate glass. The units are probability per mm of range. (Camden)

Figures 3, 4, and 5 show the integral distribution in range of electrons in Schott D263M glass, PEEK, and POLYIMIDE, respectively. The ordinate scale is per-cent per mm.

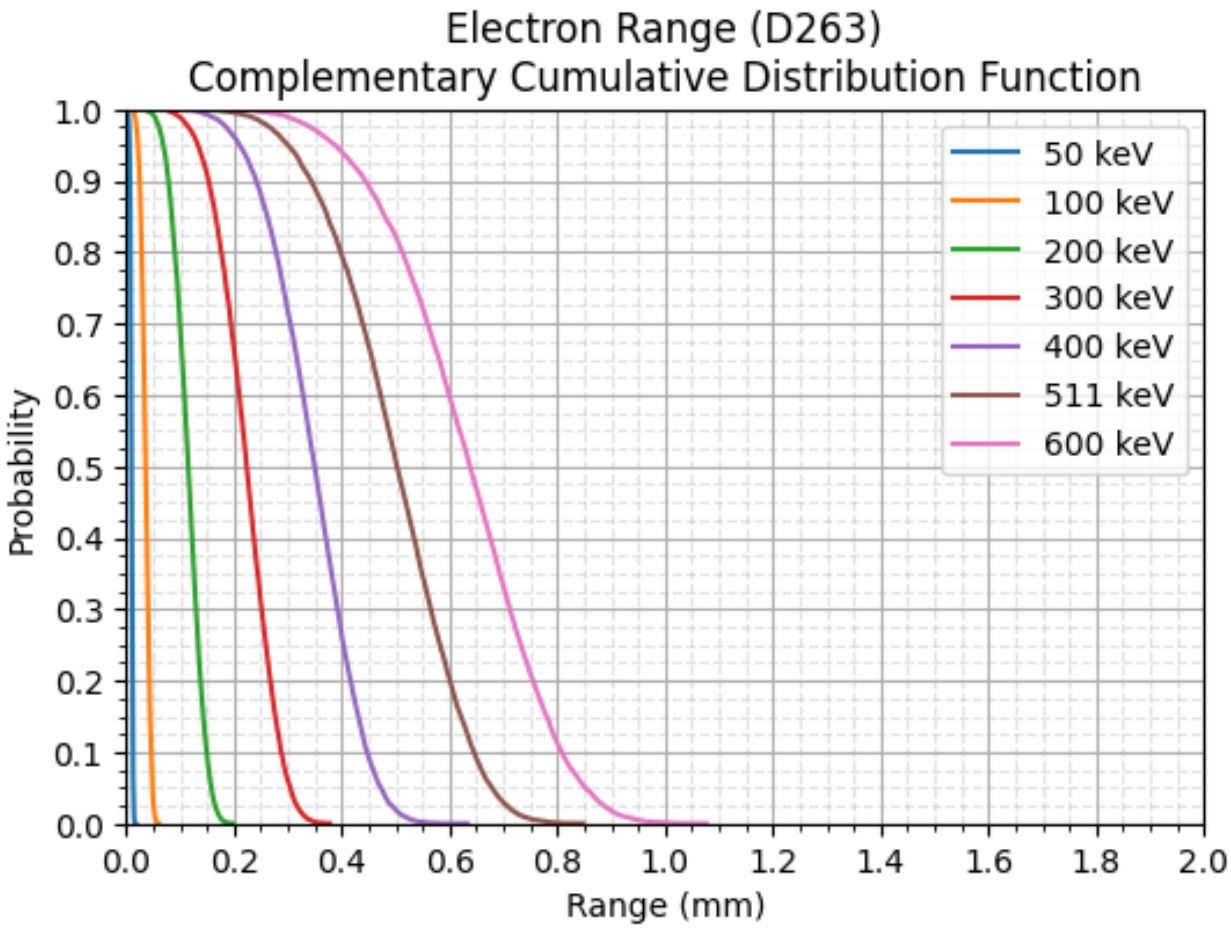

Figure 3: The integral distributions in range of electrons in Schott D263M. The units are probability per mm of range. (Camden)

2.4 Substrate Thicknesses for 90%Electron Range at Normal Incidence

Table 2.4 gives the substrate thickness corresponding to a 90% efficiency for an electron of a given energy and normal incidence to reach the surface on the other side.

Some comments:

1. Averaging over the electron incident angle will decrease the required lamina thickness by less than $\sqrt{2}$;
2. The plastics are thicker for the same efficiency, and so require fewer laminae and are easier to assemble;
3. All of these substrates are 'light', i.e. have long conversion lengths for the gammas. Loading the plastics and heavy glasses still need to be compared.

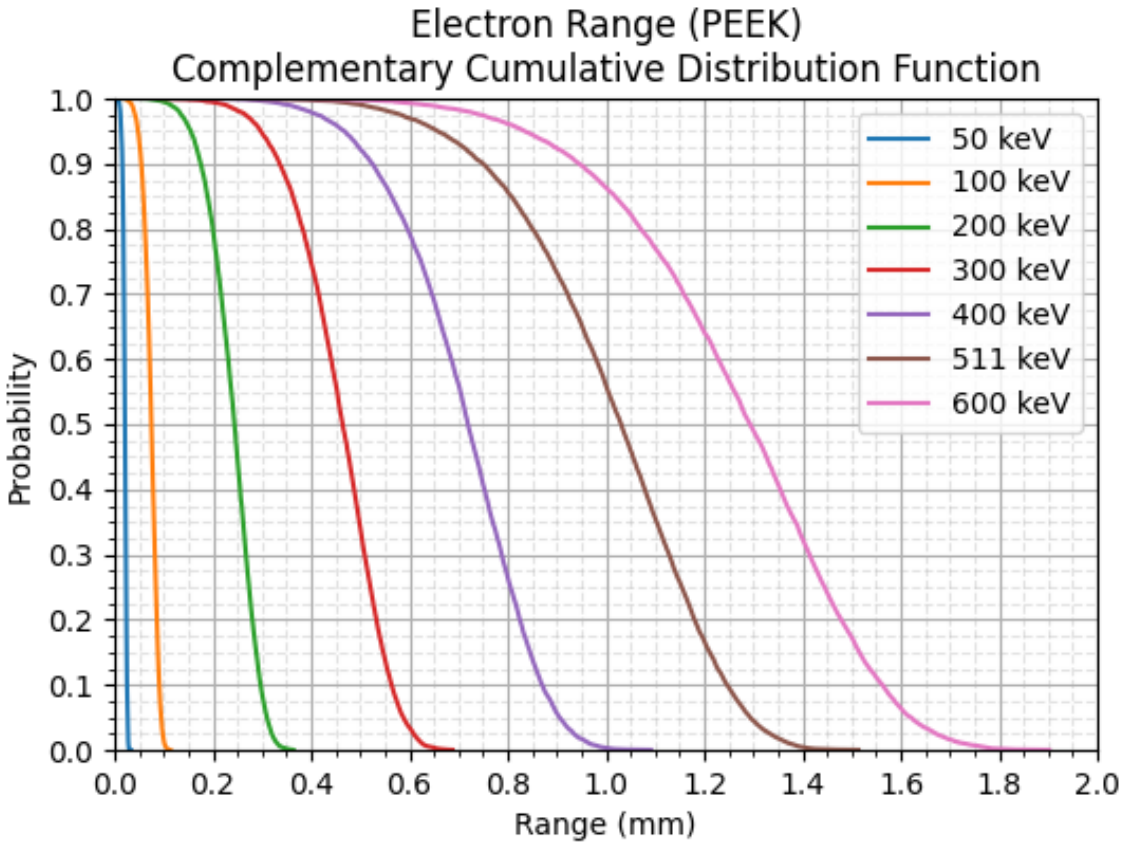

Figure 4: The integral distributions in range of electrons in PEEK. The units are probability per mm of range. (Camden)

Material	50 keV	100 keV	150 keV	200 keV	300 keV	400 keV	Comment
Polyimide	25 μm	88 μm	175 μm	285 μm	541 μm	837 μm	Dupont
PEEK	25 μm	91 μm	183 μm	297 μm	564 μm	870 μm	
D263M	13 μm	46 μm	93 μm	150 μm	280 μm	447 μm	Schott
Fused Silica	TBD	TBD	TBD	TBD	TBD	TBD	UnivWafer?

Table 3: A table of the electron range in microns for 90% efficiency for electrons with energies from 50 keV to 400 keV in candidate materials for the lamina substrate. The range corresponds to the thickness of the laminae for an electron traveling normal to the slit; the average material traversed is larger, and depends on the angles of the incoming and outgoing gammas.

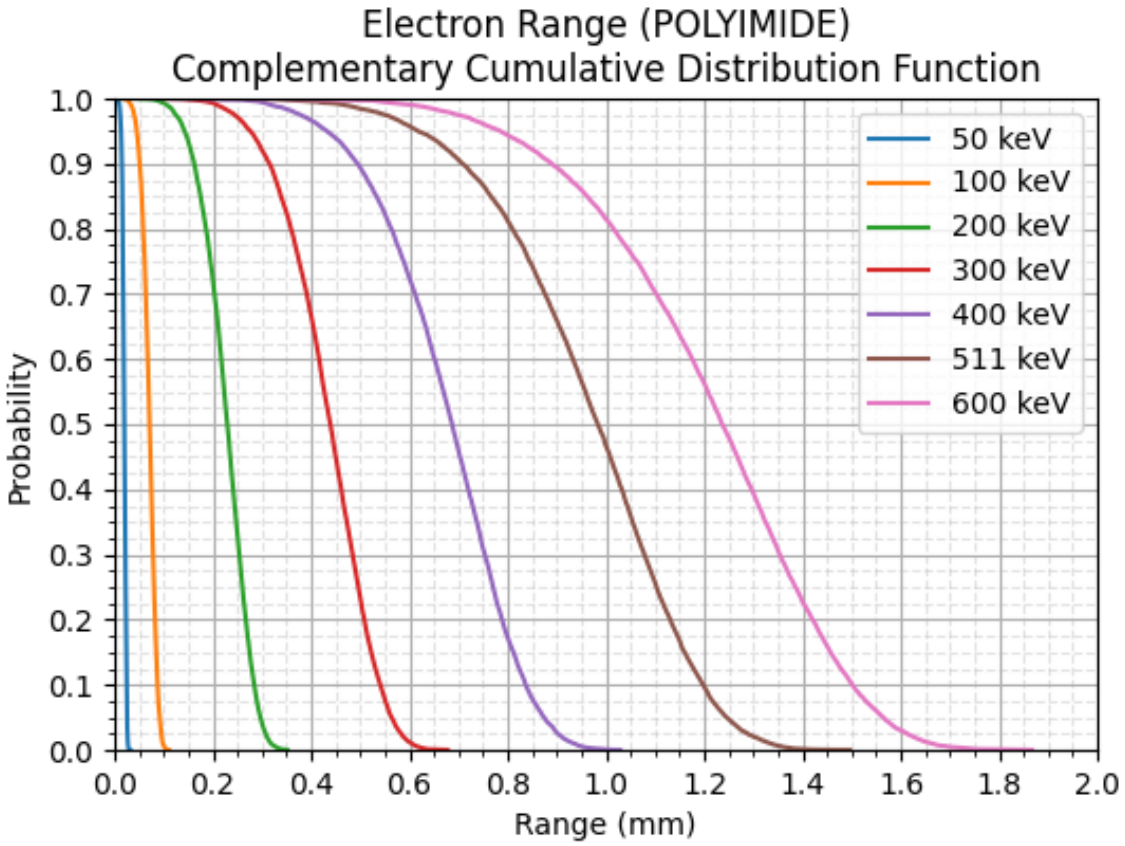

Figure 5: The integral distributions in range of electrons in POLYIMIDE. The units are probability per mm of range. (Camden)

2.5 Efficiency Plots for the Primary Electron To Cross a Channel Wall Versus Lamina Thickness

Figure 6 shows the efficiency for the primary electron created by a 511 keV gamma ray to cross at least one channel wall versus the lamina thickness, τ, for both B33 and polyimide (kapton) lamina.

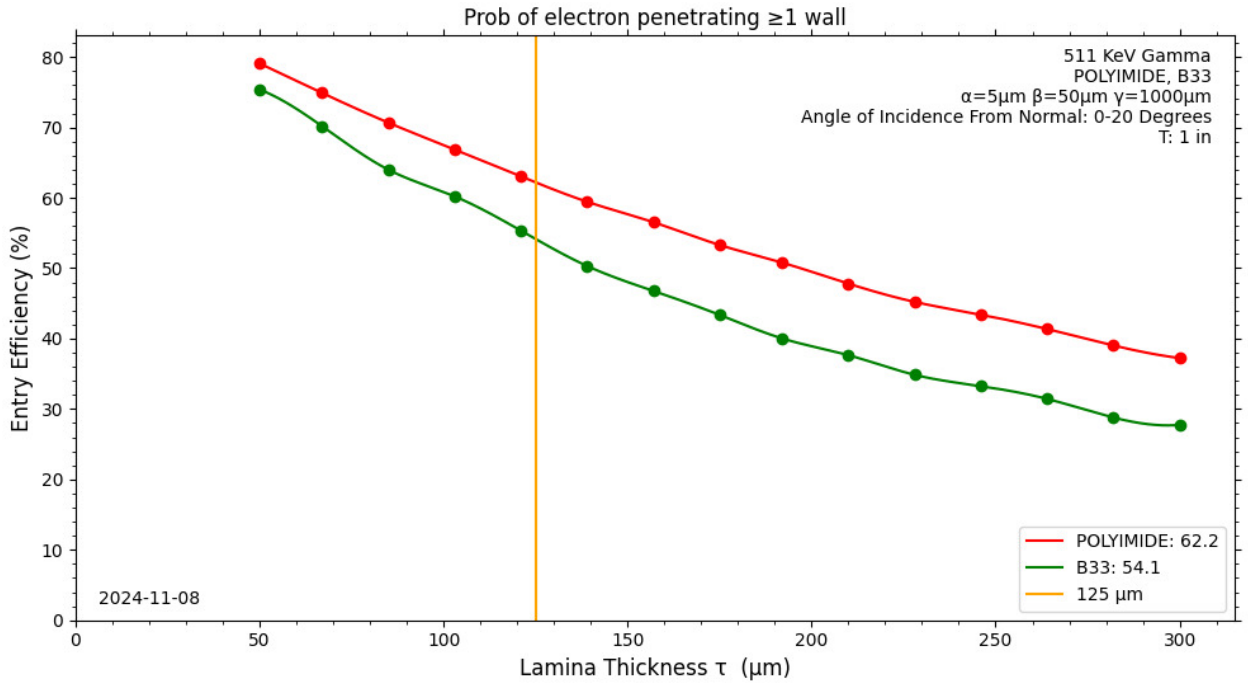

Figure 6: The efficiency for the primary electron created by a 511 keV gamma to cross at least one channel wall for a 5-micron (α) slit, vs the lamina thickness, τ in microns for B33 and polyimide lamina substrates. The yellow vertical line indicates a 5-mil thick Kapton lamina, for which this efficiency is 62.2%. (Claudio)

3 The Simple Slit MCP

The Laminar MCP (LMCP) is a proposed micro-channel plate constructed from thin laminae each with patterned channels[2] on the surface [1]. When the laminae are stacked to form a 'slab', much like books on a shelf or microscope slides in a box, the channels run from the top surface of the slab to the bottom surface, as do the pores in a conventionally constructed MCP [1].

Figure 7 defines the parameters α, β, and γ that define the channels in the LMCP, where α is the depth of the channel, β is the width of the 'wall' between channels, and γ is the width of a channel. At present we do not yet know the efficiency for the primary electron to produce a secondary electron as it enters the channel from the substrate, and so we take as our figure of merit the efficiency of the primary to cross the pore surface from the substrate into the channel.

Smaller pores (channels) provide better time resolution, important to particle and secondary-vertex identification in particle physics, among other applications [20, 21]. Photek

[2]We use the word 'channel' rather than 'pore' as the the LMCP construction method allows them to have many different geometries, coatings, and functions beyond those in conventional drawn MCPs.

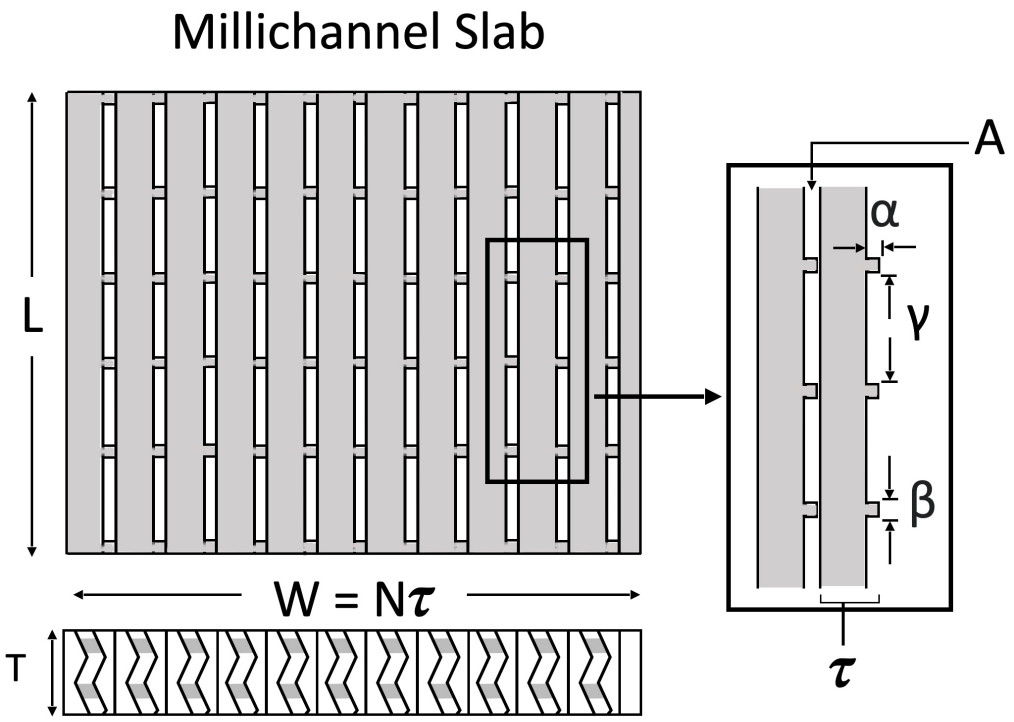

Figure 7: A 'slab' intended for gamma ray detection made from a heavy-metal dielectric such as lead-glass [1]. The slab is formed from parallel laminae of thickness τ, width T, and length L, with ridges of height α. Laminae are stacked on edge such that the ridges form channels between the laminae. The bulk laminae, which represent the largest fraction of the area of the slab, serve to convert the incoming gamma ray to an electron. The zig-zag pattern in the channels is purely for illustration of new channel geometries made possible by the access to the channel faces.

has demonstrated a pulse rise-time of 60 psec in an MCP with 2-micron pores, in principle offering the possibility of sub-ps resolution [22]. A channel having one very small dimension, i.e. a 'slit', is expected to function as a small pore once the shower has more than a few electrons, as the probability for any one electron not to hit a wall within a few slit widths is geometrically small, and so the probability that none will hit within several slit widths will be small. Once the shower has truly started, the geometric loss should be constant and negligible.

However, shower development along the slit direction may be larger than across the slit as gamma is appreciably larger than alpha. Here we suggest 500 microns (0.5 mm) as a starting value for gamma in the simulations. Even if the shower fills the channel uniformly by spreading out within a distance gamma, the rms value is $500/\sqrt{12} \approx 150$ microns. Simulation will address the lateral spreading in the gamma direction; if the spread is due to electrons and is stochastic, the scale may be set by alpha, in which case the spread of the centroid of the shower may be far less than determined by the the width gamma.

Moreover, with respect to the lateral spreading, note that the electric field will accelerate the shower down the channel rather than horizontally along the slit.[3]

[3]A question for student literature searches and simulation is if photons, immune to the field, play any role

3.1 Proposed Parameters

The 'slit' LMCP proposal is to reduce α to be as small as surface electrical uniformity for shower development and manufacturing tolerances allow, β is not critical and needs only to be robust as a spacer, and γ is large compared to α.

Parameter	Goal	Nominal (Kapton)	Description
α	1	5	Channel depth
β	10	50	Spacer ('wall') width
γ	100	500	Channel width
τ	120-240	125	Lamina thickness
T	N/A	1"	Slab/lamina height

Table 4: Slit channel parameters for the 5 mil Kapton implementation (see Fig. 1). All numbers are in microns (μm) except the slab thickness, T, which corresponds to the width of the finished Kapton tape substrate, and which here is taken as 1 inch. Multiple MCP's with independent anode readouts can be stacked above each other within the slab thickness T, improving timing and depth resolution. The 'nominal' values are set to be large for prototype manufacturability; they could be decreased with experience.

3.2 A HighRes Gamma Multiplier Tube (HGMT) Comprising a Single Layer of CLMP and ALMCP

Depending on the application, the laminae may require chamfering or other treatments on the edges for shower development and also inter-lamina connections. As an example, an architecture for an HGMT with a single Converter LMCP (CLMCP) followed by an Amplier LMCP (ALMCP) is shown in Figure 8. The ALMCP slit inputs are configured as troughs by beveling the 'upper' edge of the laminae. The ALMCP lamina are aligned with the the CLMCP lamina so that the charge cloud emerging from the slit of the CLMCP is 'funnelled' into the ALMCP slit, providing a large effective Open Area Ratio (OAR). The chamfering may also be required for making HV and HV-Ground (HVG) connections to the laminae.

3.3 The Slit Converter LMCP (CLMCP)

The CLMCP is a detector in which a gamma converts to the primary electron. As such, it should have a small open-area-ratio (OAR). Because the gamma can convert at any depth in the CLMCP and the resulting primary electron may penetrate the channel boundary over a wide range of depth in the channel, the intrinsic time resolution is poor, and the gain will vary. These two effects can be respectively ameliorated by multiple copies of a thinner CLMCP, and following each CLMCP with an ALMCP run in saturation. An alternative implementation would comprise multiple anodes in each CLMCP.

Taking some 'typical' values of the slit parameters, the OAR is given by:

in the lateral shower development for the low work-function SEY coatings we will be considering.

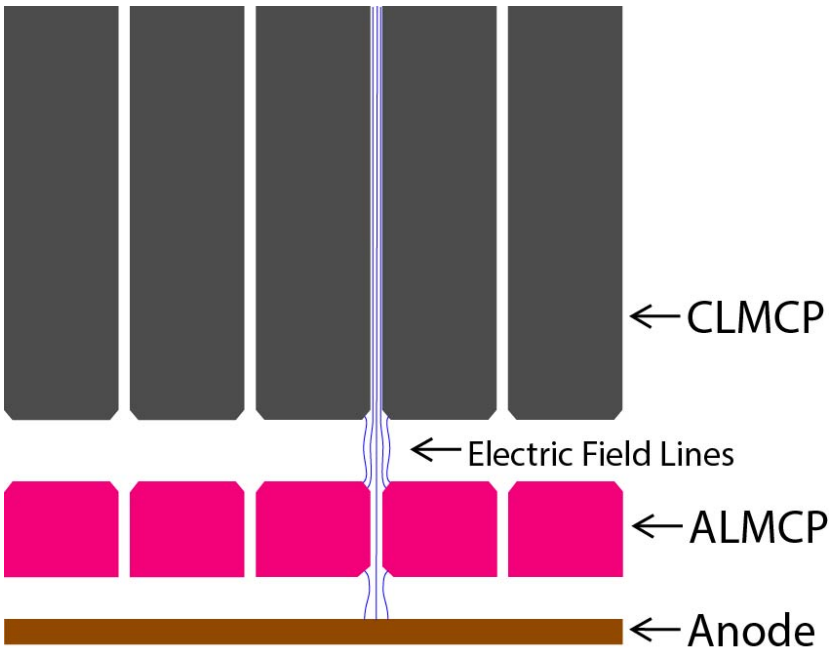

Figure 8: An elevation sketch of the architecture of a HiRes Gamma Multiplier Tube (HGMT) implemented by slit LMCPs for both the Amplifier (ALMCP) and the Converter (CLMCP) stages. The ALMCP slit input is configured as a trough, located directly below the exit of the CLMCP, providing a large effective Open Area Ratio (OAR) as the charge cloud emerging from the slit of the CLMCP is funnelled into the ALMCP slit. (Claudio)

$$\begin{aligned} OAR &= 1 - (\frac{\tau - \alpha}{\tau})(\frac{\gamma}{\beta + \gamma}) \\ &\quad - 1 - (\frac{160 - 1}{160})(\frac{1000}{10 + 1000}) \\ &= \quad 1.000 - 0.984 = 0.016 \end{aligned} \tag{1}$$

i.e., less than 2% open area, and the same fraction of enclosed vacuum in which the gamma does not convert.

3.4 The Slit Amplifier LMCP (ALMCP)

The amplifier MCP, ALMCP, follows the CLMCP to provide saturation of the pulse, as the pulse height from the CLMPC depends on the depth at which the shower starts.

The ALMCP requires a large OAR, as incoming electrons otherwise will bounce off of the top surface. The Slit LMCP with its sub-few-percent OAR may not seem ideal; however, the 1-dimension narrow nature of the slit allows chamfering the entrance edge of both sides of each lamina, forming a trough that acts as a funnel. A 10nm electrode along the crest of the trough results in an OAR of 94% in the regions above a channel. In the case where the ALMCP slits are not fed from those of a CLMCP as shown in Figure 8 a focusing wire grid parallel to the slits may substitute.

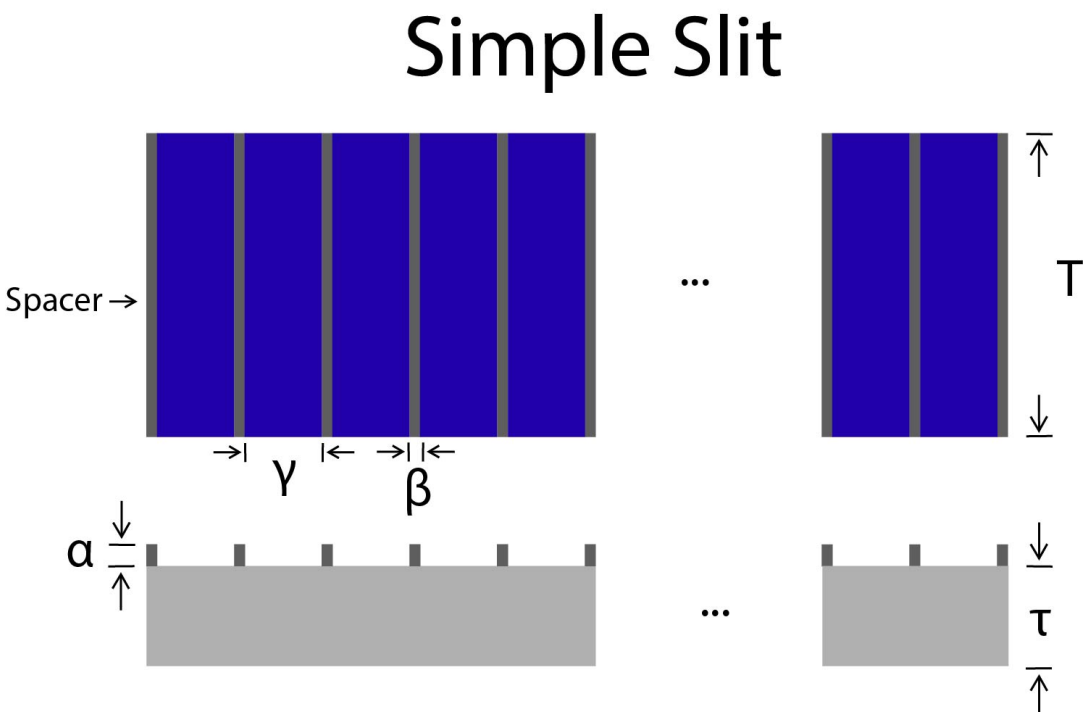

Figure 9: The front face of a 'simple' slit lamina with channels defined by physical spacers. The channel depth (slit gap) is α, typically $2 - 10\mu$m . The channel width is γ, the distance between the spacers, here typically 1-2 mm. Table 4 is a list of the target values of the lamina parameters and dimensions. (Claudio)

Figure 9 shows a lamina for a 'simple' slit LMCP in which the channels are defined by the physical walls of the spacers and have a width gamma set by the spacer pitch. Both front and back faces are coated with the resistive layer. Here the coating is shown as covering the whole face, including under the spacers. The assumption is that the anode is a separate subsystem as in the current LAPPD.

4 Integrated-Anodes and Stacked Multiple MCPs

Anodes composed of RF strip-lines have proven to be an economical high-bandwidth readout for large areas with sub-mm resolution in both transverse directions and time resolutions measured in psec [8, 9, 17].

The laminar construction of MCPs enables integrating the anode into the MCP slab, rather than have the slab source the electron shower across a vacuum gap onto a separate anode system of pads or strips. The slit LMCP design should allow the implementation of multiple anode structures on the substrates as an integral part of the additive fabrication process.

Figure 10 shows a lamina with horizontal metal traces at the end of the resistive channel forming a 50-ohm anode RF stripline on which the field lines end. With a 5 micron slit, an anode consisting of a 10 micron trace of 4-micron-thick Cu on the lamina front face

opposing (i.e. across the slit) a wider but otherwise similar ground plane on the back of the neighboring lamina gives 50-ohm impedance. For readout, the transmission line would have the far end unterminated to run in the single-ended mode used with the LAPPD anodes. To further reduce the channel count while retaining sub-mm resolution, the anode traces of 'sub-modules' of a number of laminae could be daisy-chained into a single transmission line forming one channel.

A similar structure of traces could be used to form 'last dynodes' to provide a pulse of opposite polarity for fast timing, as is often done with conventional PMTs in which both the anode and last dynode feed connectors on the back of the tube base.

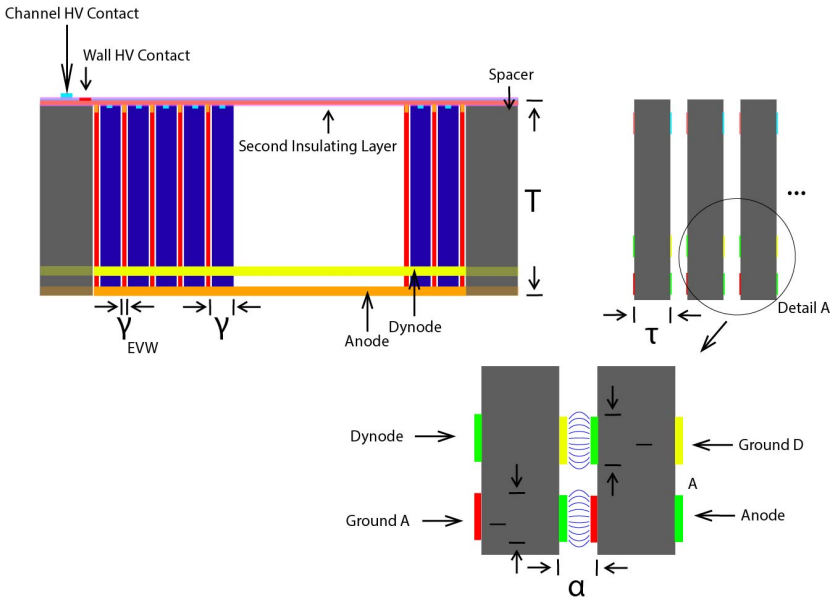

Figure 10: A schematic implementation of an integrated dynode and integrated anode on the laminae (Apologies-the figure needs updating to the simple slit geometry from the displayed and now discarded scribed implementation of electrostatic channels). Note that a 1" of slab height (T=1") can support multiple MCPs with independent anodes, providing better timing and LOR-endpoint resolution. The anode strips are accessible in the exposed slits at the ends of the laminae. (Claudio)

5 Lamina Construction

The choice of polyimide (Kapton) for the substrate simplifies the lamina fabrication as:

1. The 5-micron deep channels may be formed by 3D printing on the tape;
2. There is no need for a barrier layer;
3. Copper traces for ground, equipotential dynodes, and anodes can be routinely printed by flex-PC fab houses; EngeniusMicro could be ideal for initial tests and protyping.
4. 5-mil (125 micron) Kapton tape is inexpensive and available in 1000' foot rolls in widths from 3"-52", and in custom orders at widths smaller than 3".

5.1 Treatment of the 'Front' and 'Back' Sides of the Lamina

The spacer pattern of channels and walls is applied only to the front side of the lamina. Both sides of the lamina are patterned with equipotential metalized dynodes and emissive coatings.

The front and back sides may additionally differ in that the front face may carry the anode trace while the back face carries the corresponding ground trace of the anode transmission line; alternatively a RF strip line with ground line may be on the same lamina.

There presumably are additional differences due to HV distribution and anode inter-lamina signal circuits, yet to be designed.

5.2 Spacers

For glass substrates, the slit geometry lends itself to making the spacers by wet etching of the channels between them. Engineering Micro has demonstrated a 5 micron etch. In this case the spacer is integral with the substrate, with no concerns about matching CTEs, long-term mechanical robustness, or flatness tolerances.

For the polyimide substrate 3D printing in principle has the resolution for the channel dimensions. Outgassing is a concern.

5.3 HV Distribution System

The HV distribution system for each MCP in the stack of MCPs consists of a connection point on the top of the slab, a pattern of horizontal metal traces across both sides of each lamina and a trace or traces that connect to the lamina channel HV busses. The HV return is a similar system on the bottom of the slab.

5.4 Resistive Layer

The resistive layer is the first active layer, deposited over both sides of the lamina. The resistance range is described in Ref. [23].

Jinseo Park has proposed eliminating the resistive layer entirely, relying instead on closely-spaced metal equipotential dynodes under the emissive layer, driven by a resistive string in analogy to the HV divider in a tube base.

5.5 Emissive Layer

The secondary electron yields for MgO and Al2O3 were carefully measured during the LAPPD development [24]. Timing resolution is dominated by fluctuations in the first several strikes in which the statistics is low; the laminar design allows a larger potential drop at the upper end of an ALMCP channel.

For tubes without a photocathode the emissive layer will determine the level of vacuum needed for a 25 year life. Careful attention to outgassing from the laminae and an adequate getter [25] hopefully may suffice.

5.6 Anode Systems

Multiple anode strips running across the resistive layer could provide better time resolution due to the smaller channel length that is sampled by each anode. The anode readout connections would be made on the end face of the lamina, i.e. the horizontal line on the face would wrap around onto the end face. The anodes need to be AC coupled. For the HV connections on the top of the lamina, the corners that are traversed by the metalization should be bevelled so that the electrical connections are robust to handling.

6 Concerns

Two major areas of concern are:

1. The secondary electron yield from the high-energy primary electron exiting the substrate into the channel. This is, unfortunately, major, and will take both theoretical understanding and experimental development.
2. Robustness against outgassing, surface contamination, and migration of material across surfaces over the needed lifetime of 20 years or more.

7 Summary

We propose a 'slit' geometry for laminar MCPs, in which the gap width, alpha, is on the order of 2-5 microns, small compared to the channel width, gamma. The slit geometry may allow multiple a as RF strip line bridging the gap. The anode systems would be used to lower the distance sampled over which a shower can start to substantially improve the detector timing. The slit geometry may have advantages in fabrication cost, detection efficiency, and time resolution over designs in which $\beta \approx \alpha$. However much work remains to be done.

8 Appendix A: Electrostatic Channels

The 'simple slit' design described above is suitable for thin semi-rigid or flexible lamina substrates such as polyimide. We have considered an alternative universe of designs based on the concept of electrostatic channels, in which the channel walls are implemented by shaping the voltage distribution substantially reducing the channel width by further functionalizing the slits with 'electrostatic virtual channels' (EVC), in which the channel walls (EVW) are formed by electrostatic potentials rather than physical walls. In one implementation, these are defined by narrow resistive strips at a more negative potential; in a more speculative implementation the EVW are formed by shaping the equipotentials of a single uniform resistive layer deposited over shaped electrically-floating thin metal traces.

The physical spacers between laminae that define the slit can then be widely-spaced, on the order of inches, simplifying substrate fabrication. The electrostatic channel design can be implemented purely additively with copper traces on the substrate.

The slit geometry enables the concept of electrostatically defined 'virtual' channels, which could produce a dense array of small channels with widths comparable to the depth α, and with no inter-channel walls. Elimination of all but a few widely-spaced physical walls that serve as physical spacers defining the slit results in a higher efficiency for the primary electron to enter a channel.

The electrostatic channel design changes manufacturing considerations, as it can be implemented purely additively with surface coatings of maximum depth α on un-machined thin substrates such as glass microscope cover-slide material. In addition, since the electrostatic channel lamina substrate needs no modification, additional materials (e.g. thin ceramic or silicon wafers) can be substrates.

8.1 Channel/Wall Field Shaping By Metal Equipotentials

The process steps above for scribing the channels and walls and making the HV connections are complicated. Here we present a (newly-hatched) scheme to eliminate them entirely by leaving the resistive layer untouched and instead directly manipulating the field distribution at the surface potential distribution on the surface by defining equipotential surfaces in the resistive layer.

The scheme is to deposit (e.g. by sputtering) multiple metal traces running horizontally across the unit cell, as shown in Figure 11 before the resistive layer is deposited. As the trace is conducting, it is an equipotential. Assume that the top edge of the lamina is (negative) HV and the bottom is HV ground. If the trace is not a horizontal line, for example a sin curve as shown, where the trace is closer to the top the electric field between the trace and the top has to be higher, as the potential drop is the same everywhere on the trace, but the distance is shorter). Similarly, where the trace is farther from the top, the electric field is lower.

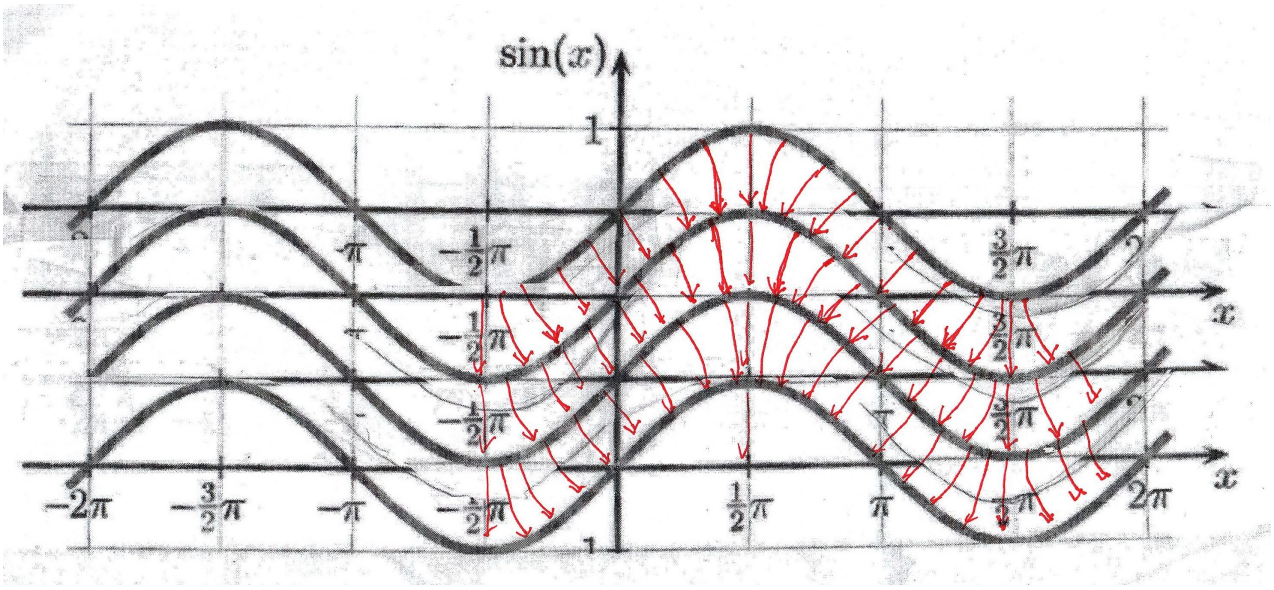

Figure 11: An example pattern of metal traces (black) on the lamina under the resistive layer to define field-shaping equipotentials that form virtual electrostatic channels and walls. The electric field lines are indicated in red.

The electric field lines connecting to a conductor are normal to the surface. If the traces are close together, where the scale parameter is the separation over the wavelength,[4] the field lines run directly from each trace to the trace below them. As the separation increases, the lines remain normal where they connect to the trace, but bow in-between. Optimization of the trace pattern will require FEA simulation.

[4]Note that the traces can be any shape; here we use sines and cosines as examples.

References

[1] K. Domurat-Sousa, C. Poe, H. J. Frisch, B. W. Adams, C. Ertley, N. Sullivan;
Surface Direct Conversion of 511 keV Gamma Rays in Large-Area Laminated Multichannel-Plate Electron Multipliers;
Nuclear Instruments and Methods; A1055, 168538 (Oct. 2023)

[2] E. Oberla and H.J. Frisch;
Charged particle tracking in a water Cherenkov optical time-projection chamber;
Nucl. Inst. Meth. Phys. Res. A814, 19 (April 2016); ISSN 0168-9002; arXiv:1510.00947

[3] K. Domurat-Sousa, C. Poe, H. J. Frisch, B. W. Adams, C. Ertley, N. Sullivan;
Low-dose TOF-PET based on surface electron production in dielectric laminar MCPs;
Nuclear Instruments and Methods; A1057, 168676 (Dec. 2023)

[4] J. Hruska and N. Sullivan;
Ultra-low-dose PET imaging for routine screening; Early detection in Oncology
To be submitted to the Journal of Nuclear Medicine.

[5] Willie Sutton was a storied 20th-centuryAmerican bank robber. When asked why he robbed banks, he replied 'Because that's where the money is.'

[6] B. Adams et al.;
A Brief Technical History of the Large-Area Picosecond Photodetector (LAPPD) Collaboration; arXiv:1603.01843

[7] S. Shin, M. Aviles, S. Clarke, S. Cwik, M. Foley, C. Hamel, A. Lyashenko, D. Mensah, M. Minot, M. Popecki, and M. Stochaj;
Advances in the Large Area Picosecond Photo-Detector (LAPPD): 8" x 8" MCP-PMT with Capacitively Coupled Readout;
arXiv 2212.03208, https://arxiv.org/abs/2212.03208

[8] F. Tang, C. Ertley, J.-F. Genat, J. Anderson, K. Byrum, G. Drake, E. May, and G. Sellberg
Transmission-Line Readout with Good Time and Space Resolutions for Planacon MCP-PMTs;
in Topical Workshop on Electronics for Particle Physics, CERN, pp. 579-583, 2008

[9] J.-F. Genat (UChicago); *Bandwidths of Transmission-Line Anodes*;
Chicago/France Workshop *The Factors That Limit Time Resolution in Photodetectors*, Session 4 *Anodes and Signal Formation*;
Univ. of Chicago; April 28-29, 2011
https://psec.uchicago.edu/workshops/fast_timing_conf_2011/.

[10] S. Ritt, *The Role of Analog Bandwidth and S/N in Timing*
Chicago/France Workshop, Session 4 *Anodes and Signal Formation*;
Univ. of Chicago; April 28-29, 2011
https://psec.uchicago.edu/workshops/fast_timing_conf_2011/.

[11] E. Angelico, T. Seiss, B. W, Adams, A. Elagin, H. J. Frisch, E. Spieglan;
Capacitively coupled pickup in MCP-based photo-detectors using a conductive, metallic anode
Nucl. Inst. Meth. Phys. Res. A. (Oct. 2016);

[12] E. Oberla and H. J. Frisch; *The design and performance of a prototype water Cherenkov optical time-projection chamber*; Nucl. Instr. and Meth. A; 814, pp 19-32. April 2016

[13] G. Drake (ANL), *Dependence on Feature Size*;
Chicago/France Workshop *The Factors That Limit Time Resolution in Photodetectors*, Session 5 *Electronics*;
Univ. of Chicago; April 28-29, 2011;
https://psec.uchicago.edu/workshops/fast_timing_conf_2011.

[14] S. Ritt, *Overview of Limitations*;
Chicago/France Workshop, Session 5 *Electronics*;
Univ. of Chicago; April 28-29, 2011
https://psec.uchicago.edu/workshops/fast_timing_conf_2011.

[15] Eric Delagnes (Saclay); *Noise*
Chicago/France Workshop *The Factors That Limit Time Resolution in Photodetectors*, Session 5 *Electronics*;
Univ. of Chicago; April 28-29, 2011
https://psec.uchicago.edu/workshops/fast_timing_conf_2011.

[16] J.-F. Genat,G. Varner, F. Tang, H. Frisch;
Signal Processing for Pico-second Resolution Timing Measurements;
Nucl.Instrum.Meth.A607:387-393,Oct., 2009.

[17] E. Oberla, J.-F. Genat, H. Grabas, H. Frisch, K. Nishimura, and G Varner
A 15 GSa/s, 1.5 GHz Bandwidth Waveform Digitizing ASIC;
Nucl. Instr. Meth. A735, 21 Jan., 2014, 452;

[18] E. Oberla; *PSEC4 Waveform Sampler & LAPPD Readout Electronics*
Talk given remotely to Workshop on Picosecond Photon Sensors, Clermont-Ferrand; 12-March 2014
UC Document Library #243, http://lappddocs.uchicago.edu/

[19] In parallel with the LMCP detector development effort we are currently designing PSEC5, a 40 GS/sec 4GHz bandwidth 8-channel low-power ASIC:
J. Park, E. Angelico, A. Arzac, D. Braga, A. Datta, T. England, C. Ertley, F. Fahim, H. J. Frisch, M. Heintz, E. Oberla, N. J. Pastika, H. D. Rico-Aniles, P. M. Rubinov, X. Wang, Y. M. R. Yeung, and T. N. Zimmerman;
Design of an 8-Channel 40GS/s 20 mW/Ch Waveform Sampling ASIC in 65 nm CMOS;
arXiv 2407.09575 (2024); https://arxiv.org/abs/2407.09575

[20] Neal Sullivan (Arradiance); *Simulation of Timing Determinants:Predictions and Results*;
Chicago/France Workshop Session 3 *Micro-Channel Plates*;

Univ. of Chicago; April 28-29, 2011
https://psec.uchicago.edu/workshops/fast_timing_conf_2011.

[21] Anton Tremsin (UCB/SSL/Arradiance) *What is Known Experimentally About Timing Determinants*,
Chicago/France Workshop Session 3 *Micro-Channel Plates*;
Univ. of Chicago; April 28-29, 2011
https://psec.uchicago.edu/workshops/fast_timing_conf_2011.

[22] J. S. Milnes and J. Howorth;
Picosecond time response characteristics of microchannel plate PMT detectors.
In 26th International Congress on High-Speed Photography and Photonics, vol. 5580, pp. 730-740. SPIE, 2005

[23] N. Sullivan et al.;
Preliminary Specifications for LMCP Substrate and Functional Coatings;
PSEC Document Library #394; http://lappddocs.uchicago.edu/

[24] Z. Insepov, V. Ivanov, S. J. Jokela, I. V. Veryovkin and A. V. Zinovev; *Comparison of secondary electron emission simulation to experiment*; Nucl. Instr. Meth A639, 155 (2011)

[25] H. J. Frisch; *Some Getter Numbers*; LAPPD Document Library Entry #325; lappddocs.uchicago.edu/documents/. Draft little note; however ST707 (70% Zirconium, 24.6% Vanadium, and 5.4% Iron) was used in the UC LAPPD prototype air=transfer 20-cm modules. A possible starting point for further investigation.